Nonlinear optical behavior of a four-level quantum well with coupled relaxation of optical and longitudinal phonons

X. Q. Luo,[1] D. L. Wang,[1] Z. Q. Zhang,[1] J. W. Ding,[1] and W. M. Liu[2]

[1]*Department of Physics & Institute for Nanophysics and Rare-earth Luminescence, Xiangtan University, Xiangtan 411105, China*

[2]*Beijing National Laboratory for Condensed Matter Physics, Institute of Physics, Chinese Academy of Sciences, Beijing 100190, China*

(Received 27 April 2011; published 2 September 2011)

We study analytically the characteristics of optical absorption and slow-light solitons in an asymmetrical four-level N configuration semiconductor quantum wells with the cross-coupling relaxation of longitudinal-optical phonons (CCRLOP). It is shown that, in the linear range, the electromagnetically induced transparency (EIT) depends on the coherence control of both the optical fields and the CCRLOP. A double EIT is obtained under a relatively strong optical field which is from the hole and antibonding states in the wide well. Especially, the double EIT becomes perfect under the condition of increasing the CCRLOP. In the nonlinear range, the CCRLOP has an important effect on both the amplitude and the group velocity of the solitons. The amplitude of solitons reveals parabolic changes which obtain a maximum value with the increase of CCRLOP. The group velocity of the solitons continuously slows down if there are fixed three-photon detunings. These results may have potential applications for all-optical switching and some optical information engineering in solid systems.

DOI: 10.1103/PhysRevA.84.033803 PACS number(s): 42.50.Gy, 42.65.Tg, 78.67.De

I. INTRODUCTION

Semiconductor quantum wells (QWs), whose discrete energy levels and optical properties are very similar to those of atomic vapors [1–4], have recently attracted considerable attention in the field of nonlinear optics. Such a system also has inherent advantages such as large electric dipole moments, high nonlinear optical coefficients, wide adjustable parameters, and flexibility. Over the past few years, there have been a large number of efforts on quantum coherence and interference effects in such QWs and coupled QW systems [5–14]. Studies on semiconductor QWs can also effectively facilitate the understanding of both the nature of quantum coherences in semiconductors and the probable implementation of optical devices based on the coherence phenomena.

Especially, electromagnetically induced transparency (EIT) has been investigated theoretically and experimentally [15–21] and gives rise to important applications in numerous processes of atomic, molecular, and solid-state systems. EIT may lead to great enhancement in nonlinear effects and steep dispersion, as well as to the reduction of group velocity and the storage of optical pulses [21,22], even under weak driving conditions. Further developments have resulted in the demonstration of highly efficient four-wave mixing [23–25], quantum phase gates [26–29], and temporal optical solitons with ultraslow propagating velocity [12,30,31]. Although the EIT effect could be created by a monochromatic field, sophisticated schemes were required to generate slow photons of different frequencies. Similarly, a bichromatic laser field may be used to acquire double EIT in atomic vapors [32–34]. For the research domains of semiconductor QWs, it is more important to focus on different processes in those media with the action of coherent optical fields, and the additional coupling optical field also plays a crucial role in optical switch devices [35]. Particularly, there is growing interest in achieving observably linear and nonlinear properties in the N configuration system, for instance, the enhancement of the Kerr nonlinearity [36], cross-phase modulation [32,37,38], dispersion switching [39,40], the possibility of superluminal propagation through coherent manipulation of a Raman process [41], and so on.

In fact, experiments report scattering rates between the electron and longitudinal-optical phonons in QWs varying from the subpicosecond range to the order of a picosecond [42,43]. To our knowledge, the cross-coupling term, which gives rise to the interference between the bonding and the antibonding states, has an important effect on the cross-phase-modulation [29] and quantum interference [35] in QW systems. Therefore, here we study how the cross-coupling relaxation of longitudinal-optical phonons (CCRLOP) affect the properties of the linear absorption and optical solitons in an N configuration QW system under Raman excitation. It is shown that a near-perfect double EIT appears with increasing CCRLOP. Also the CCRLOP can be used to determine the amplitude and the group velocity of the solitons.

This paper is organized as follows. We introduce a four-level asymmetrical double semiconductor QWs model in an N configuration system in Sec. II. Subsequently, the linear property of this system is studied in Sec. III. In Sec. IV, we derive a nonlinear Schrödinger (NLS) equation describing the evolution of the probe field and its soliton solution. Further, we discuss how the CCRLOP affects the characteristics of the solitons. A brief summary is given in the final section.

II. THE FOUR-LEVEL N CONFIGURATION SYSTEM

Based on the recent experiment condition [7,44], we consider a four-level asymmetrical double semiconductor QW in an N configuration [13,29], which consists of a wide well (WW) and a narrow well (NW) as shown in Fig. 1. In reality, the coupled QW comprises 10 pairs of a 51-monolayer (145 Å) thick WW and a 35-monolayer (100 Å) thick NW, separated by a 9-monolayer (25 Å) thick $Al_{0.2}Ga_{0.8}As$ barrier. Levels $|1\rangle$ and $|2\rangle$ (solid lines) in a valence band are localized holes states. Levels $|3\rangle$ and $|4\rangle$ (dashed lines) in a conduction band are bonding and antibonding states, respectively, which arise from the strongly coherent coupling between the two wells through the thin barrier. Such a four-state asymmetric

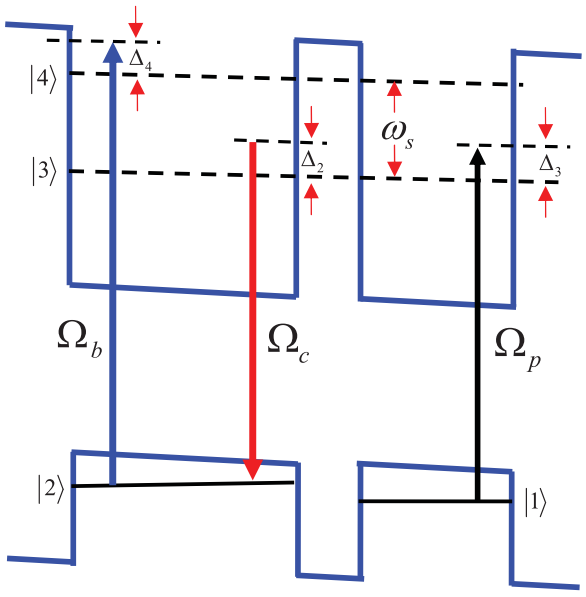

FIG. 1. (Color online) Schematic energy-level diagram and excitation scheme of an asymmetric double quantum well in an N configuration consisting of a wide well and a narrow well. Levels $|1\rangle$ and $|2\rangle$ are localized hole states of the valence band. Levels $|3\rangle$ and $|4\rangle$ are delocalized bonding and antibonding electronic states of the conduction band, which arise due to the tunneling effect between the wells via the thin barrier. Ω_p is the half Rabi frequency of the probe field; Ω_b and Ω_c are the half Rabi frequency of the control field. Δ_j ($j = 2, 3, 4$) are single-photon detunings, and ω_s is the energy interval between levels $|3\rangle$ and $|4\rangle$.

double-QW structure interacts with a low intensity, linearly polarized pulsed probe field (with half Rabi frequency $\Omega_p = \mu_{31}E_p/2\hbar$) and two strong linear-polarized continuous-wave (cw) control fields (with half Rabi frequencies $\Omega_c = \mu_{32}E_c/2\hbar$ and $\Omega_b = \mu_{42}E_b/2\hbar$), where $\mu_{ij} = \mu_{ij}\cdot\tilde{e}_L$ ($i,j = 1,2,3,4$) are the dipole moments of the transitions $|i\rangle \leftrightarrow |j\rangle$, with $\tilde{e}_L$ is the polarization unit vector of the laser field. The weak probe field with center frequency ω_p drives the transition $|1\rangle \leftrightarrow |3\rangle$, while the two strong cw control fields with center frequencies ω_c and ω_b drive the transitions $|2\rangle \leftrightarrow |3\rangle$ and $|2\rangle \leftrightarrow |4\rangle$, respectively. The electric-field vector of the system can be written as $\vec{E} = \sum_{l=p,c,b}\vec{e}_l\,\varepsilon_l\exp[i(\vec{k}_l\cdot\vec{r} - \omega_l t)] + \text{E.c.}$, where $\vec{e}_l$ ($\vec{k}_l = n_l\omega_l/c$) is the polarization direction (wave vector) of the lth field with the envelope ε_l, n_l is the background index of refraction at frequency ω_l, and c is the speed of light in vacuum. Here E.c. represents the electric field complex conjugate.

We suppose that the carrier density in the wells is so low that the many-body effects resulting from electron-electron interactions may be neglected [45]. In the interaction picture, by using the rotating wave approximation [21], the semiclassical Hamiltonian of the system is given by

$$\begin{aligned} H_I/\hbar = &-\Delta_p|3\rangle\langle 3| - (\Delta_p - \Delta_c)|2\rangle\langle 2| \\ &-(\Delta_p - \Delta_c + \Delta_b)|4\rangle\langle 4| - (\Omega_p|3\rangle\langle 1| \\ &+\Omega_c|3\rangle\langle 2| + \Omega_b|4\rangle\langle 2| + i\kappa|4\rangle\langle 3| + \text{H.c.}), \end{aligned} \quad (1)$$

where H.c. represents the Hamiltonian complex conjugate. Here $\Delta_p = \omega_p - \omega_{31}$, $\Delta_c = \omega_c - \omega_{32}$, and $\Delta_b = \omega_b - \omega_{42}$ are the one-photon detunings which denote the frequency difference between the center and the interband transitions ω_{ij} ($i,j = 1,2,3,4$) of the $|i\rangle \leftrightarrow |j\rangle$, respectively. By applying the linear Schrödinger equation $i\hbar\partial\Psi/\partial t = H_I\Psi$, with $|\Psi\rangle$ being the electronic energy state, we obtain the equations for the probability amplitude:

$$i\frac{\partial A_1}{\partial t} + \Omega_p^* A_3 = 0, \quad (2a)$$

$$\left(i\frac{\partial}{\partial t} + d_2\right)A_2 + \Omega_c^* A_3 + \Omega_b^* A_4 = 0, \quad (2b)$$

$$\left(i\frac{\partial}{\partial t} + d_3\right)A_3 + \Omega_p A_1 + \Omega_c A_2 + i\kappa A_4 = 0, \quad (2c)$$

$$\left(i\frac{\partial}{\partial t} + d_4\right)A_4 + \Omega_b A_2 + i\kappa A_3 = 0, \quad (2d)$$

with A_j being the probability of the subband state $|j\rangle$ ($j =$ 1–4) satisfying the conservation condition $\sum_{l=1}^{4}|A_l|^2 = 1$ and $d_j = \Delta_j + i\gamma_j$. Here, $\Delta_2 = \omega_p - \omega_c - \omega_{21} = 0$, indicating that the two-photon resonance is always maintained. $\Delta_3 = \omega_p - \omega_{31}$ and $\Delta_4 = \omega_b - (\omega_p - \omega_c) - \omega_{21}$ are one- and three-photon detunings, respectively. $\gamma_j = \gamma_{jl} + \gamma_{jd}$ depicts the corresponding total decay rate of level $|j\rangle$, where γ_{jl} is the population decay rate of subband $|j\rangle$, mainly due to longitudinal-optical (LO) phonon emission events at low temperature, and γ_{jd} is the dephasing decay rates of quantum coherence of the $|i\rangle \leftrightarrow |j\rangle$ transitions, determined by electron-electron scattering, phonon scattering processes, and the elastic interface roughness. The parameter $\kappa = \sqrt{\gamma_{3l}\gamma_{4l}}$ represents the cross-coupling of states $|3\rangle$ and $|4\rangle$, describing the process in which a phonon is emitted by subband $|3\rangle$ and recaptured by subband $|4\rangle$ via the LO phonon relaxation. The ratio $\zeta = \kappa/\sqrt{\gamma_3\gamma_4}$ is defined to evaluate the strength of the interference or quality of the cross-coupling of states $|3\rangle$ and $|4\rangle$. For example, $\zeta = 0$ represents no interference, while $\zeta = 1$ means a perfect interference (no dephasing). In fact, the strength of the cross-coupling between the bonding and the antibonding states can be manipulated by the dephasing rates which are realized on the basis of reducing the temperature appropriately [35,42,43].

The equation for Ω_p can be obtained by the Maxwell equation

$$\nabla^2\vec{E} - \frac{1}{c^2}\frac{\partial^2\vec{E}}{\partial t^2} = \frac{1}{\varepsilon_0 c^2}\frac{\partial^2\vec{P}}{\partial t^2}, \quad (3)$$

with $\vec{P} = N_a[(\vec{\mu}_{13}A_3A_1^* + \vec{\mu}_{23}A_3A_2^* + \vec{\mu}_{24}A_4A_2^*) + c.c]$, where c.c. represents the complex conjugate. Here N_a and ε_0 are the atomic concentration and dielectric coefficient in vacuum, respectively. Under a slowly varying envelope approximation, Eq. (3) is turned into

$$i\left(\frac{\partial}{\partial z} + \frac{1}{c}\frac{\partial}{\partial t}\right)\Omega_p + \frac{c}{2\omega_p}\left(\frac{\partial^2}{\partial x^2} + \frac{\partial^2}{\partial y^2}\right)\Omega_p + k_{13}A_3A_1^* = 0, \quad (4)$$

where $k_{13} = 2\pi N_a|\mu_{13}|^2\omega_p/\hbar c$ is the propagation coefficient. The second term in Eq. (4) depicts the transverse diffraction effect of the system. For simplicity, we assume that the probe field is homogeneous in the transverse (x and y) directions.

III. THE LINEAR PROPERTY

Here we first probe the linear properties of the system, which are the major contributors to pulse spreading and attenuation. We assume that the probe field is weak and the ground state of the system is not depleted. By setting $A_1 \simeq 1$, Ω_p and A_l $(l = 2, 3, 4)$ being proportional to $\exp[i(K(\omega)z - \omega t)]$, then substituting them into Eqs. (2) and (4), the following linear dispersion relation is obtained:

$$K(\omega) = \frac{\omega}{c} - k_{13}\frac{D_p}{D}, \tag{5}$$

where $D_p = |\Omega_b|^2 - (\omega + d_2)(\omega + d_4)$ and $D = |\Omega_b|^2 (\omega + d_3) + |\Omega_c|^2(\omega + d_4) - (\omega + d_2)(\omega + d_3)(\omega + d_4) - \kappa^2 (\omega + d_2) - i\kappa\Omega_b^*\Omega_c - i\kappa\Omega_b\Omega_c^*$. In the process of obtaining Eq. (5), we have neglected the transverse diffraction effect to leading order, which is usually very small. In most operational conditions $K(\omega)$ can be Taylor expanded around the center frequency ω_p of the probe field, that is, $\omega = 0$. We thus have $K(\omega) = K_0 + K_1\omega + \frac{1}{2}K_2\omega^2 + \cdots$, where $K_0 = \phi + i\alpha/2$ describes the phase shift ϕ per unit length and the linear absorption coefficient α of the probe field, $K_1 = dK(\omega)/d\omega|_{\omega=0}$ determines the group velocity of the probe field, and $K_2 = d^2K(\omega)/d\omega^2|_{\omega=0}$ represents the group-velocity dispersion which contributes to the shape change and the additional loss of the probe field.

To our knowledge, the imaginary part $\mathrm{Im}K(\omega)$ and the real part $\mathrm{Re}K(\omega)$ of Eq. (5) characterize the linear absorption and refractive index, respectively. So, In Figs. 2(a) and 2(b), we, respectively, plot $\mathrm{Im}K(\omega)$ and $\mathrm{Re}K(\omega)$ as a function of the frequencies ω with different control fields Ω_c. From $\mathrm{Im}K(\omega)$ in Fig. 2(a), we see that, for a low control field ($\Omega_c = 0.5$ meV), only a Lorentz line-shape absorption peak appears. This implies that the probe field with central angular frequency ω_p (corresponding to $\omega = 0$) is largely absorbed, which is similar to when the control fields are switched off (non-EIT). For a suitable middle control field ($\Omega_c = 10$ meV), the absorption profile [see the red dash-dotted curve in Fig. 2(a)] splits into two separate peaks, which is also called the Autler-Townes absorption doublet [i.e., the case of forming the EIT transparency window (TW)]. The suppression of the probe-field absorption is caused by the quantum destructive interference effect, which drives the strong control field and then renders the population in levels $|3\rangle$ and $|4\rangle$ into dark states. For a relatively strong control field ($\Omega_c = 20$ meV) [see the black solid curve in Fig. 2(a)], the TW becomes wider than that of $\Omega_c = 10$ meV. This illustrates that the width of the EIT TW can be modulated by the intensity of the control fields. Additionally, the parameters we have chosen in our numerical estimation are suitable for typical double quantum wells [13,43,44], which may provide new possibilities in current laser experiments. From $\mathrm{Re}K(\omega)$ in Fig. 2(b), meanwhile, we find that the sign of the group velocity of the probe field has changed from negative to positive with the enhancement of the control field Ω_c. This result demonstrates that it is possible to obtain double switching, in which switching from the anomalous dispersion regime to the normal dispersion regime occurs.

We also expect that both the control field Ω_b and the cross-coupling LO phonon relaxation have an influence on

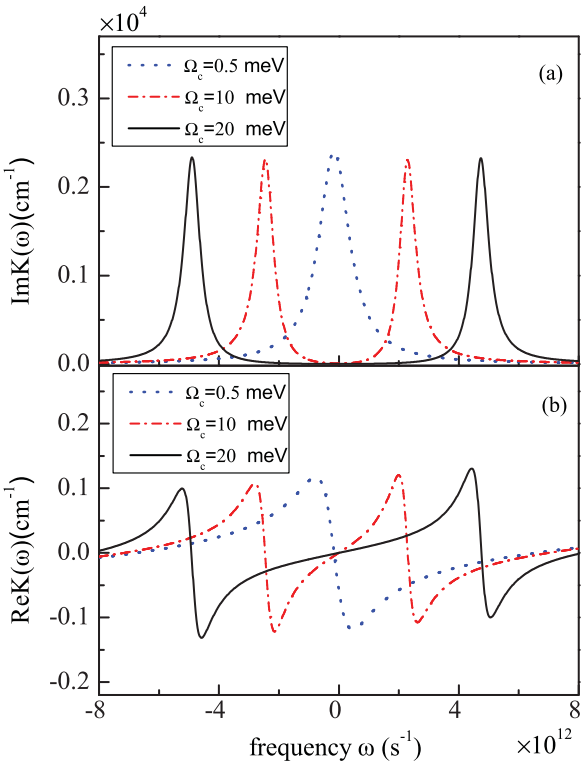

FIG. 2. (Color online) The linear dispersion relation: (a) the linear absorption $\mathrm{Im}K(\omega)$ and (b) the refractive index $\mathrm{Re}K(\omega)$ as functions of the frequency ω. The dotted, dash dotted, and solid curves correspond to the Rabi energies $\Omega_c = 0.5, 10$, and 20 meV, respectively. The other parameters used are $\Omega_b = 0.5$ meV, $k_{13} = 6.2 \times 10^3$ cm^{-1} meV, $\omega_s = 5.46$ meV, $\Delta_3 = 0.67$ meV, $\Delta_4 = 4.8$ meV, $d_2 = 0$, $\gamma_{3d} = \gamma_{4d} = 2.58$ meV, and $\gamma_{3l} = \gamma_{4l} = 2.07$ meV.

the TW width just as the control field Ω_c. We show the linear absorption $\mathrm{Im}K(\omega)$ versus the frequencies ω in Fig. 3 under a fixed control field Ω_b. From Fig. 3(a), we see that, for a relatively low control field Ω_b, there exists only a TW, which is nearly identical to the results in Fig. 2. While the cross-coupling coefficient κ increases, the width of the TW becomes narrower and the amplitude of the Autler-Townes absorption doublet decreases gradually [for clarity, also see in the inset in Fig. 3(a)]. This means that the interband excitation effectively heats the conduction electron system, and, consequently, it enhances a secondary process (i.e., the LO phonons of some possibly induce the indirect transition) in the same conduction band [46]. When Ω_b increases to 5 meV, a small peak at the center of the Autler-Townes absorption doublet appears [see the black solid curve in Fig. 3(b)]. This means that only if Ω_b increases to an appropriate value will a double EIT be able to form. Moreover, with increasing κ, the center peak increases but the amplitude of the Autler-Townes absorption doublet decreases continuously [see the red dashed curve in Fig. 3(b)]. Interestingly, when κ increases to 2 meV (which corresponds to $\zeta = 0.44$, denoting a relative strong interference between bonding and antibonding states), an approximately symmetrical three-absorption-peak configuration arises [see Fig. 3(b)]. The height of the third absorption peak dominates by the interference strength and

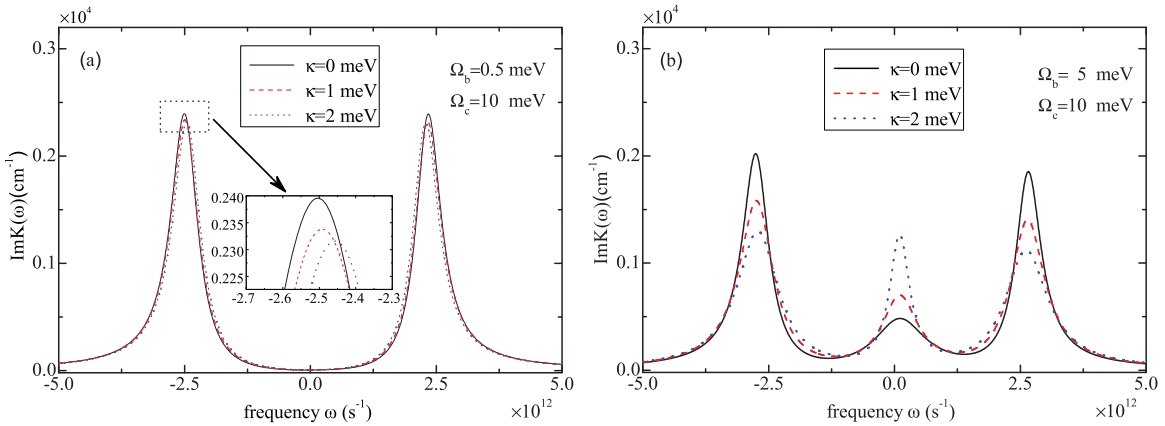

FIG. 3. (Color online) The linear absorption $\mathrm{Im}K(\omega)$ versus the frequency ω with different control fields (a) $\Omega_b = 0.5$ meV and (b) $\Omega_b = 5$ meV. The black solid, red dashed, and blue dotted curves represent cross-coupling coefficients $\kappa = 0,1$, and 2 meV, respectively. $\Omega_c = 10$ meV; the other parameters used are the same as those in Fig. 2.

can be also readily explained in accordance with dressed states [35]. This illustrates that there appears a near-perfect double EIT phenomenon under the condition of strong interference between tbonding and antibonding states in an appropriate range of the control field Ω_b.

IV. THE SLOW-LIGHT SOLITONS

We here focus on the propagation properties of a shape-preserving probe pulse, which has applications to optical transmission and information processing. Since Eq. (4) is nonintegrable, its analytical soliton solutions cannot be obtained directly. We therefore introduce a multiple-scale method [13,27,47] to study the evolution of the probe field.

First, we make the asymptotic expansions $A_1 = 1 + \sum_{j=2}^{\infty} \varepsilon^j A_1^{(j)}$, $A_l = \sum_{j=1}^{\infty} \varepsilon^j A_l^{(j)} (l = 2,3,4)$, and $\Omega_p = \sum_{j=1}^{\infty} \varepsilon^j \Omega_p^{(j)}$, where ε is a small parameter characterizing the small population depletion of the ground state. Subsequently, we assume that $A_l^{(j)}(l = 1,2,3,4)$ and $\Omega_p^{(j)}$ are functions of the multiscale variables $t_l = \varepsilon^l t$ $(l = 0,1)$, $z_l = \varepsilon^l z$ $(l = 0,1,2)$, $x_1 = \varepsilon x$, and $y_1 = \varepsilon y$. Substituting these into Eqs. (2) and (4), we have a series of equations in $A_l^{(j)}$ and $\Omega_p^{(j)}$:

$$\left(i\frac{\partial}{\partial t_0} + d_2\right) A_2^{(l)} + \Omega_c^* A_3^{(l)} + \Omega_b^* A_4^{(l)} = \alpha^{(l)}, \tag{6a}$$

$$\left(i\frac{\partial}{\partial t_0} + d_3\right) A_3^{(l)} + \Omega_c A_2^{(l)} + \Omega_p^{(l)} + i\kappa A_4^{(l)} = \beta^{(l)}, \tag{6b}$$

$$\left(i\frac{\partial}{\partial t_0} + d_4\right) A_4^{(l)} + \Omega_b A_2^{(l)} + i\kappa A_3^{(l)} = \gamma^{(l)}, \tag{6c}$$

$$i\left(\frac{\partial}{\partial z_0} + \frac{1}{c}\frac{\partial}{\partial t_0}\right) \Omega_p^{(l)} + k_{13} A_3^{(l)} = \delta^{(l)}, \tag{6d}$$

where the explicit expressions of $\alpha^{(l)}$, $\beta^{(l)}$, $\gamma^{(l)}$, and $\delta^{(l)}$ are omitted here. To leading order, one may get that $\Omega_p^{(1)} = F\exp(i\theta) = F\exp[i(K(\omega)z_0 - \omega t_0)]$, $A_2^{(1)} = [i\kappa\Omega_b^* - \Omega_c^*(\omega + d_4)]F\exp(i\theta)/D$, $A_3^{(1)} = -D_p F\exp(i\theta)/D$, and $A_4^{(1)} = [\Omega_b\Omega_c^* - i\kappa(\omega + d_2)]F\exp(i\theta)/D$, where F is a yet to be determined envelope function of the slow variable $z_l(l = 0,1,2)$ and t_1.

For the second order, a divergence-free solution requires

$$i\left(\frac{\partial F}{\partial z_1} + \frac{1}{V_g}\frac{\partial F}{\partial t_1}\right) = 0, \tag{7}$$

where $V_g = \mathrm{Re}(1/K_1)$, which means that the wave packet F propagates with the group velocity V_g.

To get the third order, the solvability condition yields the NLS equation

$$i\frac{\partial F}{\partial z_2} - \frac{K_2}{2}\frac{\partial^2 F}{\partial t_1^2} + \frac{c}{2\omega_p}\left(\frac{\partial^2}{\partial x_1^2} + \frac{\partial^2}{\partial y_1^2}\right)F - W\exp(-\bar{\alpha}z_2)|F|^2 F = 0, \tag{8}$$

with $\bar{\alpha} = \varepsilon^{-2}\alpha$, and $W = -k_{13}D_p\{|D_p|^2 + |\Omega_c|^2(|\Omega_b|^2 + |\omega + d_4|^2) + \kappa^2|\omega + d_4|^2 + [i\kappa\Omega_b\Omega_c^*((\omega + d_2)^* + (\omega + d_4)) + \mathrm{c.c.}]\}/(D|D|^2)$, where W and c.c. represent the nonlinear effect of the system and complex conjugate, respectively. Combining Eqs. (7) and (8), we obtain

$$i\left(\frac{\partial}{\partial z} + \frac{\alpha}{2}\right)U - \frac{K_2}{2}\frac{\partial^2 U}{\partial\tau^2} + \frac{c}{2\omega_p}\left(\frac{\partial^2}{\partial x^2} + \frac{\partial^2}{\partial y^2}\right)U - W|U|^2 U = 0, \tag{9}$$

where $\tau = t - z/V_g$ and $U = \varepsilon F\exp(-\alpha z/2)$. Equation (9) is a complex-coefficient NLS equation including diffraction, group-velocity dispersion, and nonlinearity. Such an equation has also appeared in the study of pulse propagation in nonlinear optical fibers and related media [48–53]. In general, such a NLS equation is still nonintegrable. If the imaginary part of the equation is much smaller than the real part, a stable soliton solution of the equation should exist. By neglecting its imaginary part, Eq. (9) is written in the following dimensionless form:

$$i\frac{\partial u}{\partial\xi} - \frac{\partial^2 u}{\partial\eta^2} + 2|u|^2 u = id_0 u + d_{\mathrm{diff}}\left(\frac{\partial^2}{\partial x'^2} + \frac{\partial^2}{\partial y'^2}\right)u, \tag{10}$$

where $\tau = \tau_0\eta, z = -2L_D\xi, d_0 = 2L_D/L_0, U = U_0 u, d_{\mathrm{diff}} = 2L_D/L_{\mathrm{diff}}$, and $(x,y) = R_\perp(x',y')$ with $R_\perp$ the beam radius. Here the characteristic dispersion length $L_D = \tau_0^2/\tilde{K}_2$ describes the effective dispersion distance of the probe field

propagation, the linear absorption length $L_0 = 2/\alpha$ depicts the effective absorption distance of the probe field, the characteristic diffraction length $L_{\rm diff} = 2\omega_p R_\perp^2/c$ represents the effective diffraction distance of the probe field, and $U_0 = \sqrt{\tilde{K}_2/\tilde{W}}/\tau_0$ is the typical Rabi frequency of the probe field based on the equilibrium condition. In order to obtain Eq. (10), we have supposed that $L_{NL} = L_D$ (where L_{NL} describes the effective nonlinearity distance of the probe field), i.e., the balance of the dispersion and the nonlinearity, for the purpose of acquiring the formation of soliton. If $d_0 \ll 1$ and $d_{\rm diff} \ll 1$, Eq. (10) can be simplified to a standard NLS equation, for which the exact soliton solution is

$$u = 2\beta \,\mathrm{sech}[2\beta(\eta - \eta_0 + 4\delta\xi)] \exp[-2i\delta\eta - 4i(\delta^2 - \beta^2)\xi], \tag{11}$$

where the real parameters β, δ, and η_0 determine the amplitude, propagating velocity, and initial position of the soliton, respectively. By setting $\beta = 1/2$ and $\delta = \eta_0 = 0$, Eq. (11) turns into $u = \mathrm{sech}(\eta)\exp(i\xi)$, so

$$\Omega_p = U \exp(i\tilde{K}_0 z) = \frac{1}{\tau_0}\sqrt{\tilde{K}_2/\tilde{W}}\,\mathrm{sech}\left[\frac{1}{\tau_0}\left(t - \frac{z}{\tilde{V}_g}\right)\right]\exp\left[i\tilde{K}_0 z - i\frac{z}{2L_D}\right], \tag{12}$$

which gives a description of a stable soliton traveling with propagation velocity V_g. Here, the quantity with the tilde means its real part, e.g., $\tilde{W} = \mathrm{Re}(W)$.

In order to explore the effect of the cross-coupling LO phonon relaxation on the properties of optical solitons, we plot in Fig. 4 the amplitude of optical solitons versus the CCRLOP with different energy level splitting ω_s. At $\omega_s = 15$ meV, one can see from Fig. 4 that with κ increasing, the amplitude of the solitons first increases and then decreases, with a maximum amplitude existing at $\kappa \approx 0.72$ ps^{-1}(where 1 ps^{-1} corresponds to 4.12 meV). Here $\zeta \approx 0.54$ denotes the relative strong interference between the cross-coupling states $|3\rangle$ and $|4\rangle$. At $\omega_s = 20$ meV, the maximum amplitude appears at

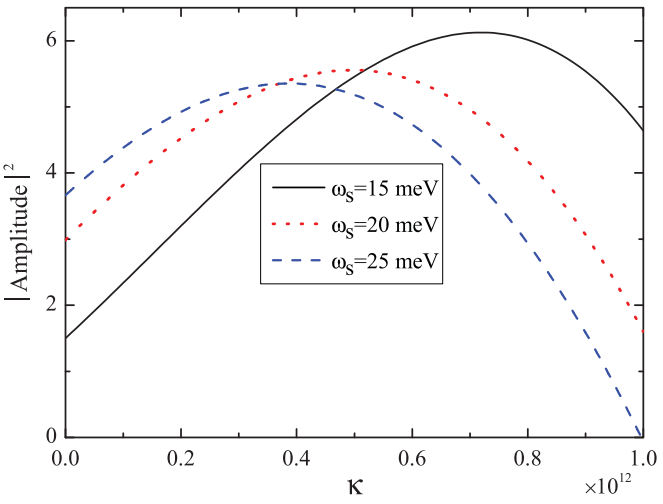

FIG. 4. (Color online) The relative amplitude of the optical solitons vs the cross-coupling coefficient κ for different energy level splitting ω_s. The other parameters used are the same as those in Fig. 2.

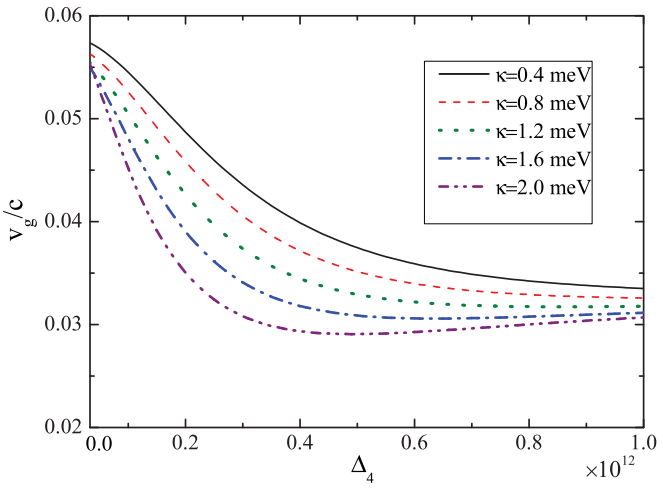

FIG. 5. (Color online) The relative group velocity of the optical solitons versus three-photon detunings Δ_4 for different cross-coupling coefficient κ. The other parameters used are the same as those in Fig. 2.

$\kappa \approx 0.5$ ps^{-1} ($\zeta \approx 0.45$; also see the red dotted curve in Fig. 4), which is smaller than that of $\omega_s = 15$ meV. When ω_s further increases to 25 meV (such as the blue dashed curve in Fig. 4), the maximum amplitude is further decreased, while its peak position is shifted at $\kappa \approx 0.36$ ps^{-1} ($\zeta \approx 0.37$). We conclude that, with κ increasing, the amplitude of the solitons first increases then decreases and an amplitude peak exists there. When the energy level splitting increases, the maximum amplitude decreases and deviates to the smaller side of the cross-coupling coefficient κ. This is because the increase of energy level splitting leads to a decrease of the spatial overlap of the cross-coupling between the bonding and the antibonding states, and then gives rise to the decrease of the soliton maximum amplitude.

We further show in Fig. 5 the relative group velocity (RGV) V_g/c as a function of three-photon detunings Δ_4 with different cross-coupling coefficients κ. One finds from Fig. 5 that for relatively small cross-coupling coefficient (e.g., $\kappa = 0.4$ and 0.8 meV, i.e., $\zeta = 0.13$ and 0.24), the RGV is nearly inversely proportional to the three-photon detunings Δ_4. At $\kappa = 1.2$ meV, with $\zeta = 0.32$, the RGV decreases sharply in the beginning stage and then approaches a constant after $\Delta_4 \approx 0.75$ ps^{-1} (3.09 meV). For a relative large κ (e.g., $\kappa =$ 1.6 meV with $\zeta \approx 0.38$), the RGV shows a visible increase after $\Delta_4 \approx 0.65$ ps^{-1}, while it exhibits a drastic decrease at the starting time. A similar phenomena can be observed when κ further increases to 2.0 meV, which corresponds to $\zeta \approx 0.44$. For a fixed Δ_4, meanwhile, the RGV of the probe field continuously decreases with increasing κ. We find that the strength of the interference between the cross-coupling states has an important effect on the soliton group velocity. For relatively weak interference ($\zeta < 0.32$), the group velocity decreases with increasing three-photon detunings Δ_4. With stronger interference ($\zeta > 0.32$), the velocity exhibits an initial decrease, which is followed by an a increase after passing through a minimum value.

V. CONCLUSION

In summary, we have studied analytically the optical absorption properties and the soliton characteristics in a four-level N configuration semiconductor QW system. We find that, in the linear case, for a suitable Rabi energy Ω_c, the system exhibits an EIT window when the Rabi energy Ω_b is properly small. And the width of transparency window can be controlled by varying the Rabi energy Ω_c. Meanwhile, double switching from the anomalous dispersion regime to the normal dispersion regime can likely be achieved by increasing the Rabi energy Ω_c under Raman excitation. Furthermore, when the cross-coupling coefficient κ increases, the width of the transparency window becomes narrower and the amplitude of the double absorption peaks decreases. Interestingly, a double EIT is achieved under a relatively strong optical field, which is from the hole and antibonding states in the wide well. In particular, a near-perfect double EIT appears under the condition of increasing the cross-coupling coefficient κ together with an appropriate range of Rabi energy Ω_b.

In the nonlinear case, it is shown that the cross-coupling coefficient κ can determine both the amplitude and the group velocity of the solitons. The amplitude of the solitons shows parabolic changes and preserves a maximum value with increasing κ. While the energy level splitting ω_s increases, the maximum amplitude decreases and deviates to the smaller side of the cross-coupling coefficient κ. The group velocity of the solitons decreases with increasing κ for fixed three-photon detunings Δ_4. For relatively weak interference, the group velocity decreases with an increase of three-photon detunings Δ_4. For strong interference ($\zeta > 0.32$), the velocity initially declines then rises after reaching a minimum value.

ACKNOWLEDGMENTS

This work was supported by NSFC under Grant Nos. 10874235, 10934010, 60978019, 11074212, 10874089, 51032002, the NKBRSFC under Grant Nos. 2009CB930701, 2010CB922904, 2011CB921502, 2011AA050526, NSFC-RGC under Grant Nos. 11061160490 and 1386-N-HKU748/10, and the Foundation for the Author of National Excellent Doctoral Dissertation of China (Grant No. 200726). We acknowledge useful discussions with Dr. Han Zhang.

[1] M. O. Scully and M. S. Zubairy, *Quantum Optics* (Cambridge University Press, Cambridge, England, 1997).
[2] H. C. Liu and F. Capasso, *Intersubband Transitions in Quantum Wells: Physics and Device Applications* (Academic, New York, 2000).
[3] S. E. Harris, Phys. Today **50**(7), 36 (1997).
[4] S. E. Harris and L. V. Hau, Phys. Rev. Lett. **82**, 4611 (1999).
[5] A. Imamoglu and R. J. Ram, Opt. Lett. **19**, 1744 (1994).
[6] J. Faist, F. Capasso, C. Sirtori, K. W. West, and L. N. Pfeiffer, Nature (London) **390**, 589 (1997).
[7] W. Pötz, Phys. Rev. Lett. **79**, 3262 (1997).
[8] P. C. Ku, F. Sedgwick, C. J. Chang-Hasnain, P. Palinginis, T. Li, H. L. Wang, S. W. Chang, and S. L. Chuang, Opt. Lett. **29**, 2291 (2004).
[9] M. D. Frogley, J. F. Dynes, M. Beck, J. Faist, and C. C. Phillips, Nat. Mater. **5**, 175 (2006).
[10] J. H. Wu, J. Y. Gao, J. H. Xu, L. Silvestri, M. Artoni, G. C. La Rocca, and F. Bassani, Phys. Rev. A **73**, 053818 (2006).
[11] J. H. Li, Phys. Rev. B **75**, 155329 (2007).
[12] W. X. Yang, J. M. Hou, and R. K. Lee, Phys. Rev. A **77**, 033838 (2008).
[13] C. J. Zhu and G. X. Huang, Phys. Rev. B **80**, 235408 (2009).
[14] G. B. Serapiglia, E. Paspalakis, C. Sirtori, K. L. Vodopyanov, and C. C. Phillips, Phys. Rev. Lett. **84**, 1019 (2000).
[15] H. Schmidt, K. L. Campman, A. C. Gossard, and A. Imamoglu, Appl. Phys. Lett. **70**, 3455 (1997), and references therein.
[16] M. Phillips and H. L. Wang, Phys. Rev. Lett. **89**, 186401 (2002).
[17] L. Silvestri, F. Bassani, G. Czajkowski, and B. Davoudi, Eur. Phys. J. B **27**, 89 (2002).
[18] T. Li, H. L. Wang, N. Kwong, and R. Binder, Opt. Express **11**, 3298 (2003).
[19] M. C. Phillips, H. L. Wang, I. Rumyantsev, N. H. Kwong, R. Takayama, and R. Binder, Phys. Rev. Lett. **91**, 183602 (2003).
[20] Y. Wu and X. X. Yang, Phys. Rev. A **71**, 053806 (2005).
[21] M. Fleischhauer, A. Imamoglu, and J. P. Marangos, Rev. Mod. Phys. **77**, 633 (2005).
[22] C. Liu, Z. Dutton, C. H. Behroozi, and L. V. Hau, Nature (London) **409**, 490 (2001).
[23] L. Deng, M. Kozuma, E. W. Hagley, and M. G. Payne, Phys. Rev. Lett. **88**, 143902 (2002).
[24] D. A. Braje, V. Balic, S. Goda, G. Y. Yin, and S. E. Harris, Phys. Rev. Lett. **93**, 183601 (2004).
[25] Y. P. Zhang, B. Anderson, and M. Xiao, Phys. Rev. A **77**, 061801 (2008).
[26] X. Y. Hao, L. G. Si, C. L. Ding, P. Huang, J. H. Li, and X. X. Yang, J. Opt. Soc. Am. B **27**, 1792 (2010).
[27] C. Hang, Y. Li, L. Ma, and G. X. Huang, Phys. Rev. A **74**, 012319 (2006).
[28] C. Ottaviani, D. Vitali, M. Artoni, F. Cataliotti, and P. Tombesi, Phys. Rev. Lett. **90**, 197902 (2003).
[29] W. X. Yang and R. K. Lee, Opt. Express **16**, 17161 (2008).
[30] M. M. Kash, V. A. Sautenkov, A. S. Zibrov, L. Hollberg, G. R. Welch, M. D. Lukin, Y. Rostovtsev, E. S. Fry, and M. O. Scully, Phys. Rev. Lett. **82**, 5229 (1999).
[31] Y. Wu and L. Deng, Opt. Lett. **29**, 2064 (2004).
[32] M. Paternostro, M. S. Kim, and B. S. Ham, Phys. Rev. A **67**, 023811 (2003).
[33] G. Q. Yang, P. Xu, J. Wang, Y. F. Zhu, and M. S. Zhan, Phys. Rev. A **82**, 045804 (2010).
[34] S. J. Li, X. D. Yang, X. M. Cao, C. H. Zhang, C. D. Xie, and H. Wang, Phys. Rev. Lett. **101**, 73602 (2008).
[35] J. H. Wu, J. Y. Gao, J. H. Xu, L. Silvestri, M. Artoni, G. C. La Rocca, and F. Bassani, Phys. Rev. Lett. **95**, 57401 (2005).

[36] H. Sun, S. Q. Gong, Y. P. Niu, S. Q. Jin, R. X. Li, and Z. Z. Xu, Phys. Rev. B **74**, 155314 (2006).
[37] Z. B. Wang, K. P. Marzlin, and B. C. Sanders, Phys. Rev. Lett. **97**, 63901 (2006).
[38] H. Sun, Y. P. Niu, R. X. Li, S. Q. Jin, and S. Q. Gong, Opt. Lett. **32**, 2475 (2007).
[39] X. M. Hu, G. L. Cheng, J. H. Zou, X. Li, and D. Du, Phys. Rev. A **72**, 023803 (2005).
[40] H. Kang, L. L. Wen, and Y. F. Zhu, Phys. Rev. A **68**, 063806 (2003).
[41] G. S. Agarwal and S. Dasgupta, Phys. Rev. A **70**, 023802 (2004).
[42] T. Asano, S. Noda, T. Abe, and A. Sasaki, Jpn. J. Appl. Phys. **35**, 1285 (1996).
[43] A. Neogi, H. Yoshida, T. Mozume, and O. Wada, Opt. Commun. **159**, 225 (1999).
[44] H. G. Roskos, M. C. Nuss, J. Shah, K. Leo, D. A. B. Miller, A. M. Fox, S. Schmitt-Rink, and K. Köhler, Phys. Rev. Lett. **68**, 2216 (1992).
[45] D. E. Nikonov, A. Imamoglu, L. V. Butov, and H. Schmidt, Phys. Rev. Lett. **79**, 4633 (1997).
[46] M. Cardona and R. Merlin, *Light Scattering in Solids. IX, Novel Materials and Techniques* (Springer, New York, 2007).
[47] Y. C. She, D. L. Wang, W. X. Zhang, Z. M. He, and J. W. Ding, J. Opt. Soc. Am. B **27**, 208 (2010).
[48] Y. S. Kivshar and G. P. Agrawal, *Optical Solitons: From Fibers to Photonic Crystals* (Academic, San Diego, 2003).
[49] H. Zhang, D. Y. Tang, L. M. Zhao, and X. Wu, Phys. Rev. B **80**, 052302 (2009).
[50] A. Hasegawa and M. Matsumoto, *Optical Solitons in Fibers* (Springer, Berlin, 2003).
[51] W. M. Liu, B. Wu, and Q. Niu, Phys. Rev. Lett. **84**, 2294 (2000).
[52] H. Zhang, D. Y. Tang, L. M. Zhao, and X. Wu, Phys. Rev. A **80**, 045803 (2009).
[53] A. C. Ji, X. C. Xie, and W. M. Liu, Phys. Rev. Lett. **99**, 183602 (2007).